Spectrograph Stabilization Method using a Single-delay Interferometer on the Hale Telescope

David J. Erskine[a], Jerry Edelstein[b], Martin M. Sirk[b], and Ed H. Wishnow[b]

[a]Spectral Fringe, Oakland, CA, USA
[b]Space Sciences Lab, University of California, Berkeley, CA 94720, USA

ABSTRACT

We describe a technique for spectrograph stabilization useful when conventional mitigation techniques of vacuum tanks, thermal insulation and laser frequency comb may be impractical, expensive, heavy, or bulky. This includes spectrographs on airborne platforms, or mounted on telescopes where they suffer a changing gravity vector or other drifts. Placing a fixed-delay interferometer in series with a spectrograph forms an Externally Dispersed Interferometer (EDI). This produces a uniform sinusoidal comb multiplying input spectrum, creating (through heterodyning) beats (moiré patterns). In Fourier space for low frequencies up to the comb frequency, the moiré generated signal counter-rotates to ordinary spectra under an unknown disperser wavenumber drift Δx. This generates a large negative feedback signal useful in a conceptual control loop, to converge rapidly to a stable spectrum and yield Δx. A modified EDI data analysis algorithm ("crossfading") combines frequency-weighted moiré with conventional spectrum, to cancel net output spectrum reaction to Δx. Needing only a single-delay, this is a practical improvement over prior crossfading analyses requiring multiple delays. We test crossfading on ThAr data near 4850 cm^{-1} taken on Hale telescope in an earlier project. In a single pass we reduce drift 20 times. Using 7 iterations, we reduce 0.5 cm^{-1} (31 km/s Doppler equivalent) drift to 4x10^{-7} cm^{-1} (2.5 cm/s). The interferometer delay can wander, since linearity of phase vs wavenumber interpolates science features between bracketing calibrating spectral references. Secondly, mathematically reversing the heterodyning effect doubles effective spectral resolution without changing disperser slit.

Keywords: High-resolution spectroscopy, spectrograph stabilization, interferometric frequency comb

1. INTRODUCTION

An interferometer in series with a dispersive spectrograph creates a hybrid instrument EDI,[1–16] which can dramatically enhance the performance of a disperser used alone. (The EDI technique has been used by other researchers to discover exoplanets[17–19] around HD102195 and HD87646, as well as confirmation of 51 Peg.[20]) We have explored several EDI applications: Doppler radial velocimetry of M stars,[8,9] and high resolution spectroscopy.[6,7,10,11,21]

1.1 Synopsis

This proceedings describes a new EDI application, called "crossfading", useful for the spectroscopy community, which is a variation on the mathematics to process EDI data. This mathematical method to analyze fringing spectra can stabilize the output spectrum to unknown and irregular wavelength shifts in the disperser component, and yield the value of the offset, and the spectrum, when both are initially unknown.

In a EDI, there are two sources of information for the unknown spectrum: the ordinary nonfringing component (ie the conventional disperser output), and the fringing component. They are independent. Since they are independent, it is useful to play one against the other to learn the offset that affects the nonfringing signal more strongly than the fringing.

The two signals are obtained from the set of (at least three) phase stepping exposures, by adding and subtracting in two different linear equations (see Appendix). (Equivalently, one can fit the data using a sine

Author information:
D.E.: derskine@spectralfringe.org

fit algorithm along phase axis. The intensity offset yields the ordinary nonfringing spectrum, and the sine and cosine amplitudes yield the imaginary and real parts of the complex fringing spectrum, for each pixel along the dispersion axis.) The crossfading style of analyzing the data, in effect, is a high quality manner of using or combining both signal types at their best. The low spatial frequencies are handled mostly by the ordinary signal, since they are strongest there, and the higher spatial frequencies mostly by the fringing signal, since they are not only strongest there but they are most robust to disperser shifts.

In fact, at the very specific spatial frequency which is the interferometer periodicity, the fringe phase of a spectral lamp line feature is independent of disperser wavelength error– you can open up the spectrograph slit very wide, up until it starts to encompass other lines, and shift the wavelength position slightly and the fringe phase is unchanged. And the fringe phase is used to determine the output wavelength (λ) or wavenumber ($\nu = 1/\lambda$) of that feature.

However, that amazing robustness to disperser drift is only at that very specific Fourier frequency. Since an arbitrary spectrum has an arbitrary distribution of Fourier frequencies, what happens to the output spectrum when there is a disperser shift (unknown to the user) and all the spatial frequencies are involved, but in some complicated way? The crossfading method is a way of handling that issue in a manner that is mathematically sound. Not the only way, since there are a manifold of allowed choices on the weightings when combining signals, but a reasonable way.

This crossfading data analysis method does not require a stabilized interferometer, since the interferometer transmission sine comb phase offset (used to heterodyne against the stellar input spectrum) is determined by absolute spectral references such as a ThAr spectral lamp. This is a software/math advance rather than a hardware advance. We have demonstrated this technique[14,16] on previously measured EDI data taken at the Hale telescope in the 2011 time frame, which suffers from drifts in the TripleSpec NIR spectrograph.[22] The method is described by a recent US patent[15] held by Lawrence Livermore National Laboratory.

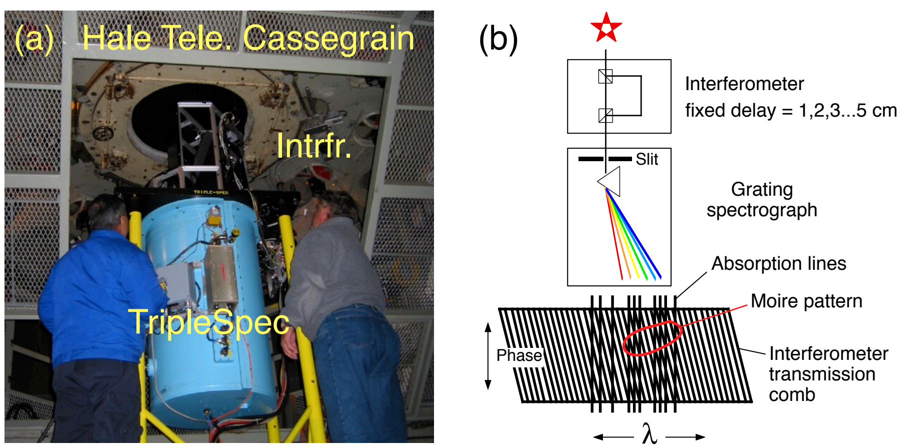

Figure 1. (a) TripleSpec spectrograph (blue cryostat) with T-EDI interferometer (black and silver) above, attaching to Cassegrain output of 5m Hale Telescope at Mt. Palomar, 2007-11. (b) EDI scheme—a fixed delay interferometer crossed with disperser. Figure reproduced with permission from Ref. 10 by SPIE.

1.2 Apparatus: EDI in series with TripleSpec spectrograph at Hale telescope

Our EDI work[9–11] at the Hale telescope used the TripleSpec NIR spectrograph[22] as the disperser component (Fig. 1). This shows EDI mounted above a TripleSpec[22] spectrograph (blue dewar) at the Cassegrain output of 5m Hale Telescope.

1.3 Problem: irregular disperser drift Δx

Figure 2 shows example irregular spectrograph wavelength drift measured on TripleSpec spectrograph. The observed drift is challenging because it changes polarity and magnitude on short distance scales of 2 cm^{-1}. A significant problem is there are no nearby spectral reference lines over this region in which to calibrate away the irregular wavelength shifts.

2. SOLUTION: STABILIZATION USING PAIRS OF SIGNALS

2.1 Stabilization using pairs of fringing signals

Previously[14] we theoretically explored another EDI application: combining processed fringing signals from different delays to stabilize the net output spectrum against unknown and irregular drifts Δx in the disperser (the TripleSpec). This was a new mathematical technique for processing multiple-delay EDI data, which we call "crossfading", after how a sound engineer gradually fades out one audio source and fades in another while maintaining nearly a constant net volume.

The crossfading (X-EDI) data analysis algorithm modifies how we mathematically combine signals of pairs of partially overlapping delays, noting that under a drift Δx, the low frequency half of the higher delay reacts oppositely in phase to higher frequency half of lower delay (Fig. 15 of Ref. 14). By strategically choosing frequency dependent weights, the net reaction to Δx of overlapping delays can be made zero or very small. This is a mathematical advance that re-analyzed older EDI data having multiple delays, and achieved dramatic results[14] of ∼1000x times less change in output peak position drift than with disperser used alone.

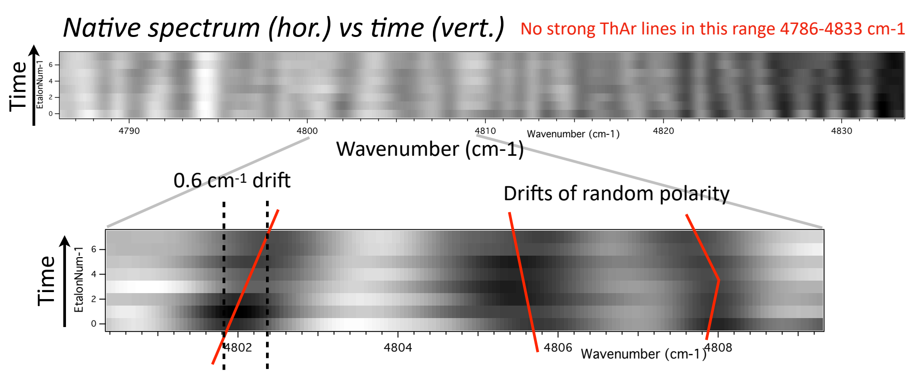

Figure 2. Example irregular spectrograph wavelength drift measured on TripleSpec[22] used with T-EDI.[9–11] Each row is HD219134 conventional spectrum at a different time. (Quasi-periodic lines are a telluric feature– an additive white light comb was not used). Observed drift is difficult because it is bipolar irregular in magnitude (∼0.6 cm^{-1}), changes over a small distance scale of 2 cm^{-1}, and no strong ThAr lines are within this range 4786-4833 cm^{-1} to calibrate. Figure reproduced with permission from Ref. 10 by SPIE.

2.2 Stabilization using native plus single fringing signal

More recently, we wondered if crossfading stabilization could also work with a single delay, rather than multiple delays, by substituting the ordinary (native) spectrum for lower delay signal, and using the single delay as higher delay. This is an algorithm extension. The answer is yes, it works!

The purpose of present paper is to re-analyze Triplespec-EDI data using only a single delay (of eight available), to demonstrate this new method extension. Since a single delay is the most common interferometer configuration, this is a practical improvement. It is a mathematical and software advance, not a change in hardware from the classic EDI.

3. BACKGROUND

3.1 Conventional mitigations

Spectrographs are used everywhere in science, engineering, medicine, forensics, and remote sensing for national security. Dispersive spectrographs spread the spectrum spatially across a detector and use positional changes to determine wavelength (distance from reference or calibration line). Some spectrographs cannot be perfectly

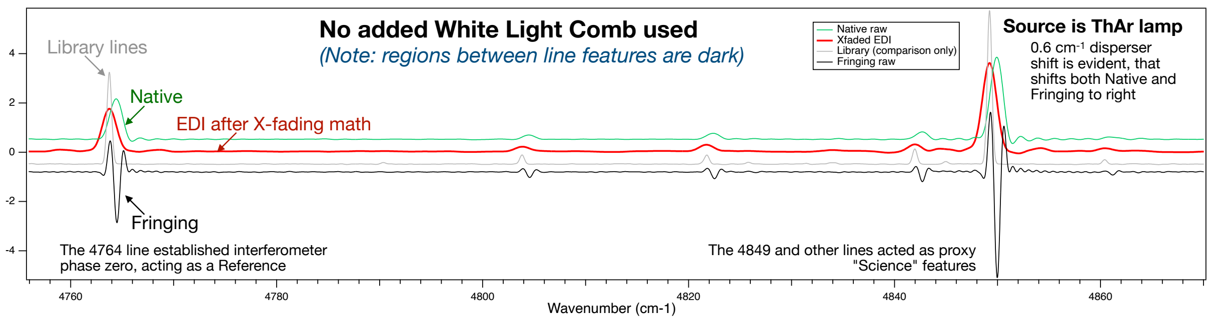

Figure 3. Demonstration of crossfading stabilization on a ThAr spectral lamp data. Evidence that crossfading EDI does not use an additive white light comb, since it would appear between ThAr line features, and we observe darkness. This is because our sine comb "ruler" is multiplicative, not additive. The 4764 cm^{-1} ThAr line and its library[23] (gray) position established interferometer phase zero. Other library lines are not used for computations. Large line at 4849 cm^{-1} and smaller lines elsewhere are proxy "science" features demonstrating crossfading correction (red) compared to drifted native (green). Curves vertically offset.

rigid or isothermal, which can cause a wavelength error. This can be corrected by a spectral reference (i.e. ThAr lamp) if features with absolutely known features are near to the science features. However when the reference is too far away from science features to constrain the wavenumber versus pixel function, an error can persist, which is the case for our TripleSpec data (Fig. 2).

Conventional mitigations such as vacuum tanks, fiber optic scramblers and exquisite thermal control are conventionally used to reduce drifts, but these mitigations can be heavy, expensive and preclude mobile use on airborne or spaceborne platforms, or on the rotating telescope itself due to excessive weight or bulk.

A uniform grid of a laser frequency comb (LFC) can calibrate spectrographs, but only if they have sufficiently high resolution to resolve LFC spike spacing, big enough budget to support the cost, space for the LFC apparatus and its environmental controls, and manpower to tend to its operation. (For example, our EDI at Hale had insufficient resolving power (∼2700) to resolve LFC spike period, even if we had the budget for it.) References 24 and 25 describe HARPS performance using a LFC, and Ref. 26 surveys observatory spectrograph performance.

For exoplanet Doppler and direct measurement of cosmic redshift drift,[21,27] spectrographs need to be ultra-stable—an incredible 1/30,000 pixel rigidity is needed to characterize an Earth-like planet (∼10 cm/s stability). Cosmic redshift drift measurements require multi-year measurements– a length over which detectors can fail. Replacement detectors can have different pixel placement, potentially producing a wavelength error. (The EDI's insensitivity to detailed pixel position is an advantage here).

3.2 Stable monolithic interferometers used by others

Some researchers use white light sine combs added to the input spectrum to calibrate their data. Our Hale EDI apparatus did not use additive sine combs. Instead we use a multiplicative sine comb to explore the resolution boosting and stabilization ability afforded by the heterodyning action.

References 28–32 describes thermally stable monolithic interferometers (SMI) developed by other researchers, using two glasses (BK7 and LAK7) having different thermal responses to cancel net drift. A useful application of an SMI is to illuminate it with white light to create a sinusoidal white light comb (WLC), which can be added as a calibrant to an input beam to a spectrograph system– analogous to a LFC, but which can have a selectable and lower density of features suitable for lower resolution spectrographs.

Our crossfading EDI does not use an additive WLC calibrant. This is evident in data of a ThAr lamp shown in Fig. 3 by the lack of a sinusoid in the dark space between ThAr lines. Instead, the EDI's sinusoidal transmission function multiplies not adds against the input (stellar or ThAr) spectrum. This produces a heterodyning action that is useful, both for effectively boosting spectral resolution beyond the disperser used alone, but also producing the negative feedback signal in fringe phase (for low spatial frequencies below the comb frequency) that is central to the crossfading stabilization method we describe.

Our crossfading EDI interferometer at the Hale telescope was not of monolithic type. This was to allow easy selection of free standing etalons (fused silica) mounted on an 8-position wheel to change the delay. The placement of the interferometer optics in the Cassegrain output hole surrounded by a 5-meter glass mirror provided natural temperature stability. The TripleSpec spectrograph, housed in a liquid nitrogen dewar and subject to a changing gravity vector, likely suffered greater environmental stresses than our interferometer, nestled in the cavity above it. The unstable wavelength drifting of the TripleSpec is demonstrated in data of Fig. 2.

Malitson[33] measured fused silica dn/dT of $\sim$11x10^{-6} per °C at 1 μm and Hahn[34] the coefficient of thermal expansion (CTE) as 0.5x10^{-6}, but the dn/dT dominates, yielding $\sim$0.1 cycle phase shift per °C.

Note that for our EDI at the Hale telescope the short term thermal delay wandering would be much smaller than the $\sim$1 cycle commanded phase shift via PZT transducer (over a dataset of 5 min)– hence the stable delay of SMI was not required for our application. (For long term it would have been convenient, but still not required, since the absolute delay was measured spectroscopically via ThAr spectral lamp.)

3.3 Articles describing crossfading stabilization method

A journal article submitted to JATIS describes in detail[16] our recent extension of the crossfading technique to use of a single-delay crossfading method. It is also described by recent US Patent[15] 12,480,815 held by Lawrence Livermore National Laboratory. An older article[14] describes multiple-delay crossfading method, which shares many of the same mathematical operations as the current single-delay method. The roots of the technique appear in Sections 9.4 and 10 of a 2016 JATIS article[10] on data analysis of EDI at the Hale Telescope. A follow up JATIS article[11] explores how photon and detector noises propagate through the two signal components, fringing and native. Figure 8 of that reference discusses how uncorrelated they might be despite being derived from the same set of phase stepped exposures.

4. CROSSFADING METHOD THEORY

4.1 Low frequencies move in opposition

Figure 4 illustrates that the low and high frequencies halves of an EDI wavelet reacting oppositely to each other. And significantly, low frequencies move oppositely to the native spectrum disperser drift Δx!

This creates a correcting signal to cancel the drift in the native spectrum. The low frequencies manifest a large negative feedback signal useful in a conceptual control loop, to converge rapidly to a stable spectrum and yield Δx.

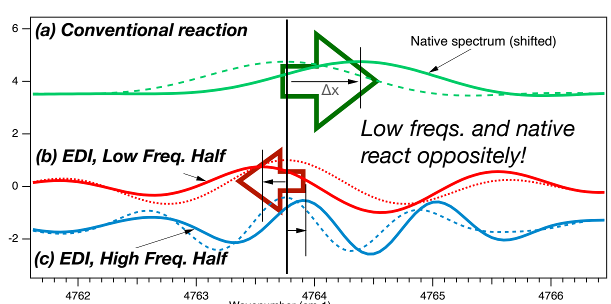

Figure 4. Illustration in ν of low and high frequencies halves of EDI wavelet reacting oppositely to Δx (dashed/dotted to bold curves). (a) Native (green) has direct reaction $\Delta\nu = \Delta x$. (b)(c) EDI frequencies split into (b) low (red) and (c) high (blue) wavelets (at $\rho = \tau$) react oppositely, confirming polarity flipping of reaction line in ρ-space. Significantly, (b) low frequency wavelet reacts oppositely to Δx. This is means zero net reaction to Δx if native and low frequencies are combined strategically.

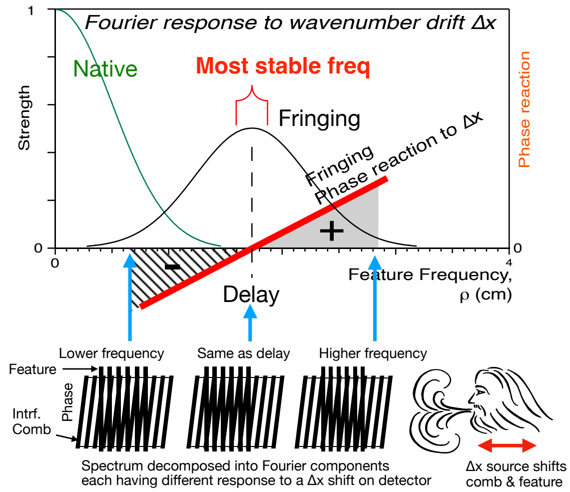

Figure 5. (Top) frequency-space (Fourier-space) illustration of classic EDI, having single delay τ but ignoring native spectrum. Fringing phase reaction line (red line) crosses zero at peak center $\rho = \tau$, the most stable frequency, since it's moiré is flat and immune to Δx. However, arbitrary spectra contain a range of frequencies. Crossfading algorithm is stable over a range. (Bottom) moirés having different slants at different ρ. Translation of moiré (wind icon) by Δx evokes different polarity reactions vs ρ.

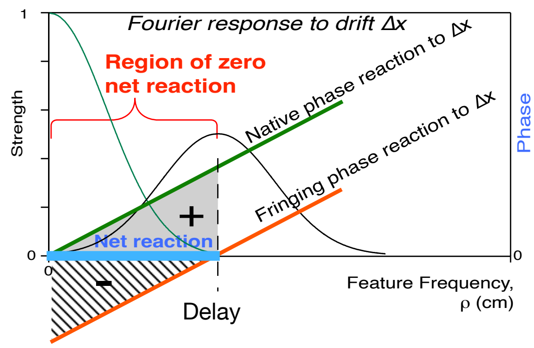

Figure 6. Crossfading scheme using a single fringing peak overlapping native peak. Under Δx the two signal types have opposite phase reactions for $\rho \leq \tau$. Combining using ρ-dependent weightings, native (green) and fringing (red) reactions cancel (blue thick line having zero phase vs ρ).

4.2 Goal: combine low frequency fringes & native spectrum

Figure 5 shows frequency-space (Fourier-space) illustration of classic EDI, having single delay τ but ignoring native spectrum. This shows in frequency (ρ) space how lower frequencies have opposite phase reaction to a drift Δx. The red line is the phase reaction to Δx.

Figure 6 shows the crossfading scheme in Fourier-space. The green line passing through the origin is the phase reaction line for the native (ordinary) spectrum. A key point is that for frequencies $0 < \rho < \tau$, e.g. below the delay or interferometer comb frequency, the fringing phase reaction is opposite the native phase reaction, and thereby we can potentially cancel the net phase reaction by adding those two signals. This works provided the frequency dependent weights (ie. filtering) are chosen strategically, so that for each frequency bin cancellation occurs.

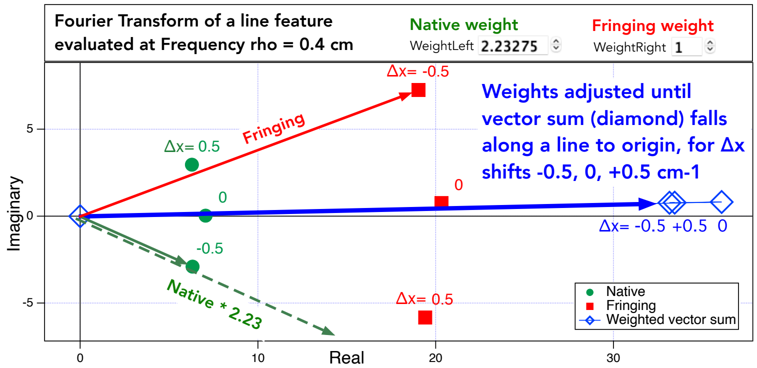

Figure 7. Geometric construction screen in our software, used to find optimal weight ratios, here for $\rho = 0.4$, so that sum vector (blue open diamonds) of native (green circles) and fringing (red squares) vectors changes minimally for Δx = -0.5, 0 and +0.5 cm^{-1}. This indicates that sum phase is independent of Δx, ie. stable. Vectors are complex values of Fourier transform of a ThAr line, for native (green), and E3 delay of fringing (red). Results for all ρ are in Table 1.

5. IMPLEMENTATION OF CROSSFADING

5.1 Choosing weights by observing reaction of displaced ThAr line

To compute desirable frequency dependent weights applied to the two signals, fringing and nonfringing (native), we first analyze how a ThAr lamp line reacts to a wavenumber displacement Δx, but observed in Fourier space. We use measured data and our regular data analysis software, and deliberately translate input data by a selectable Δx. Since Fourier values are complex, they can be represented by a vector in the complex plane (Fig. 7). The angular (phase) of the Fourier value, rather than its magnitude, is the most important for establishing the wavenumber position of a feature. So we desire the sum (blue vector) of the fringing vector (red) and native vector (green), be insensitive to changes in Δx.

Figure 7 shows a screenshot of our software window where we choose weights, for a given frequency, to produce an insensitivity of the sum vector angle while Δx changes from 0 to 0.5 to -0.5 cm^{-1} (blue open diamonds). For frequency of 0.4 cm shown, the choice of 2.23x for native weight produces a constant angle of the blue sum vector (indicated by alignment of the three blue open diamonds pointing to the origin). For simplicity we kept the fringing weight at unity, since only the ratio of weights matters here. We used this method to find native weights for frequencies ranging from 0 to 0.6 cm (near the delay value), with results shown in Table 1. This process is described in more detail in Sect. 8.7 of Ref. 14, and in the submitted JATIS journal article.[16]

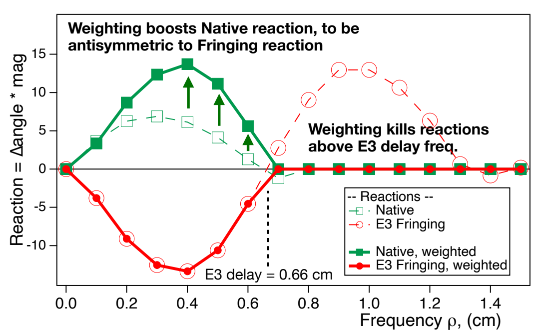

Figure 8. Angular reaction curves. Effect of multiplying chosen ρ-dependent weights of Table 1 against raw data (open circles & squares) is to form curves with solid markers. This makes reaction of native curve (bold green) more antisymmetric to fringing curve (bold red), to improve cancellation when they are summed. Frequencies above E3 delay ($\rho > 0.66$ cm) are deleted, since they have same polarity and do not cancel. These are displacement reactions of the "calibration" ThAr peak at 4764 cm^{-1}, for etalon E3 (0.66 cm) (red curve) and native (green curve), using $\Delta x = 0.5$ cm^{-1}.

Table 1. Relative weights for each frequency ρ (0 to 0.7 by 0.1 cm) which satisfies vector cancellation, for native spectrum (middle) and fringing delay E3 (right). Only ratio between middle and right values matters, since later equalization multiplies both.

Frequency (cm)	Weight of native	Weight of delay E3
0	1	0
0.1	0.915	1
0.2	1.386	1
0.3	1.792	1
0.4	2.233	1
0.5	2.700	1
0.6	4.370	1
0.7	0	0

Since the angular (phase) component of the Fourier value is the most important to stabilize against Δx, it is useful to plot in Fig. 8 the angular reaction, which is the magnitude of the vector times the angular shift, for both unweighted (open symbols) and weighted (closed symbols) cases of fringing (red) and native (green). This shows that weighting improves the antisymmetry between fringing and native case, improving the cancellation when they are summed. We also zero out both data for frequencies above delay 0.66 cm, since opposition is not possible for frequencies above the delay where the fringing reaction flips polarity but the native does not (as seen in Fig. 6).

5.2 Simulation of crossfading on a single ThAr line

Figure 9 shows simulation of single pass crossfading on 4849 cm^{-1} ThAr line,[23] using the chosen weights. Drift Δx is initially unknown. It is discovered after the first pass.

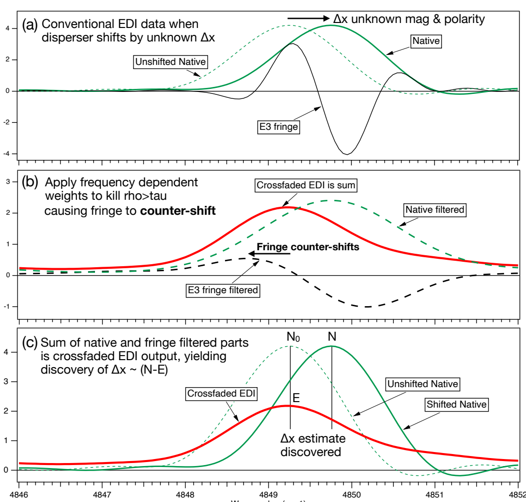

Figure 9. Simulation of single pass crossfading on 4849 cm^{-1} ThAr line under drift $\Delta x = 0.5$ cm^{-1}. (a) Shifted native (solid green) and E3 fringing (black). Unshifted native is dotted green and is unknown by algorithm. (b) Frequency dependent weight $k_0(\rho)$ [ie. filtering] applied to native (dashed green), and $k_1(\rho)$ to fringing (black dashes). This slightly broadens native peak (high frequencies suppressed), and shifts fringing peak opposite direction of Δx. (b)(c) The sum is crossfaded EDI output (bold red). (c) We compare peak position (E) of crossfaded EDI output to position N of native to form (N-E), which estimates Δx. Using (N-E) as negative feedback, we shift raw data by -Δx and repeat process iteratively from (a). Algorithm does not need initial value of Δx; after converging it outputs Δx.

6. RESULTS (SINGLE-PASS)

Figure 10 shows demonstration of single-pass crossfading correction on TripleSpec echelle spectrograph data.[10] Four data sets having independent drifts Δx, due to combination of Fiber A to B offset, plus drift over time when target star changed. Vertical alignment of bottom panel shows success. Drift has been defeated.

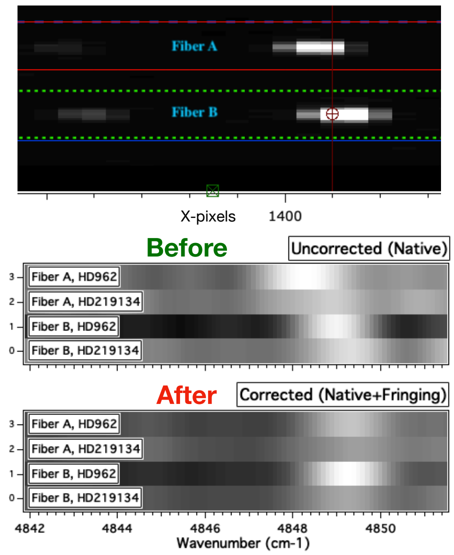

Figure 10. Demonstration of single-pass crossfading correction on TripleSpec echelle spectrograph data.[10] (Top) detector image of ThAr lamp alone– geometry of echelle optics causes ThAr line to displace ∼1 pixel, (∼0.6 cm^{-1}) between fibers A and B. (Middle, Bottom) "Before" and "After" versions of four stacks of spectrum lineouts versus wavenumber, from HD962 and HD219134 with ThAr. Four instances of Δx are sum of fiber offsets and natural drift (∼1 hour). (Bottom) "After" panel shows data processed with crossfading successfully corrects drifts– note vertical alignment of features. A 4764 cm^{-1} ThAr line (off graph) provides absolute reference[23] for interferometer phase.

Figure 11 shows stability transfer function (output offset $\Delta\nu$ vs input offset Δx), for single pass of single-delay crossfading. A single pass produces a 20x reduction of effect of drift.

Figure 12 shows demonstration of single-pass crossfading correcting bipolar irregular drift on simulated data similar to Fig. 2. Vertical alignment of bottom panel shows success. Drift has been defeated.

Figure 3 shows ThAr lamp data over a wider bandwidth, having multiple spectral lines. The crossfading operation corrects all the lines at-once. Note the darkness in between the ThAr lines. This demonstrates we do not use a white light sine comb added to the input spectrum as a calibrant. Instead we use a multiplicative sine comb (the interferometer transmission function). Multiplicative sine comb allows resolution boosting, and opposition between low and high fringing frequency phase shifts which is basis for crossfading stabilization.

7. RESULTS (ITERATIVELY)

Using 7 iterations, we reduce in simulation an initial drift of 0.5 cm^{-1} [31 km/s] 10^6 times, down to $4\text{x}10^{-7}$ cm^{-1} [2.5 cm/s]. This result has not yet been experimentally confirmed at the cm/s level.

Figure 13 shows an optional final step after Δx is discovered, all the Fringing frequencies can be used, high and low, in an optional recalculation that combines Native and Fringing but with an equalization that produces 2x resolution of the Native alone. (Note red peak is now narrower than green native peak.)

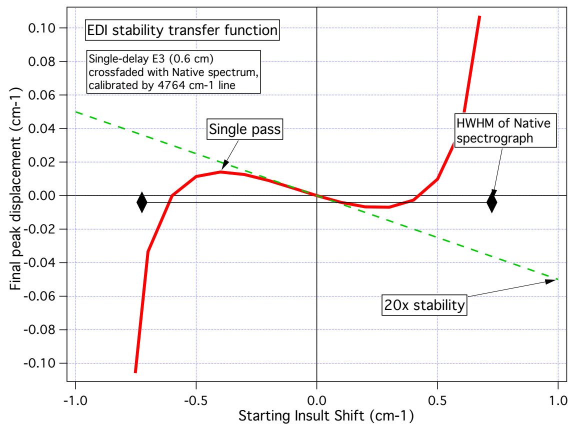

Figure 11. Stability transfer function (output offset $\Delta\nu$ vs input offset Δx), for single pass of single-delay crossfading. We used measured ThAr data, but with artificial Δx. The 4849 cm^{-1} ThAr line (our "science" line) used weighting coefficients chosen from reactions at 4764 cm^{-1} line (our "calibration" line). This shows linear regime where crossfading works is $\Delta x <\sim \pm 0.75$ cm^{-1} a distance of one FWHM of native PSF (black diamonds). Here the output $\Delta\nu$ is linear to input Δx with slope (TRC $=\Delta\nu/\Delta x$) of $\sim$0.05 (dashed green line). Hence the stability gain (reciprocal of TRC or $\Delta x/\Delta\nu$) is $\sim$20x. Iterative passes of crossfading can further improve stability by several orders of magnitude.

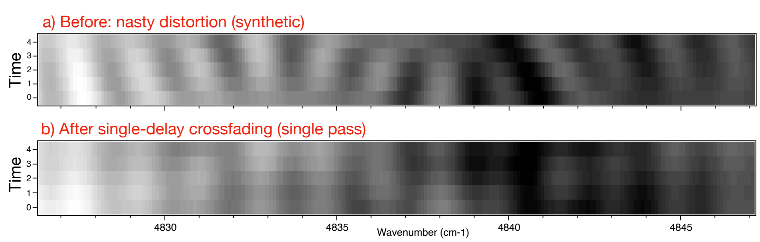

Figure 12. Demonstration of single-pass crossfading correcting bipolar irregular drift on simulated data similar to Fig. 2. (a) Input was TripleSpec[22] data (Fig. 2) artificially distorted, each row a different amount, in "M" shape between 4826 and 4846 cm^{-1}, shifting -0.6 to +0.6 cm^{-1}. (b) Result after single-pass crossfading– parallelism of features indicates success. Note that the quasi-periodic lines are a telluric feature, not an additive white light comb.

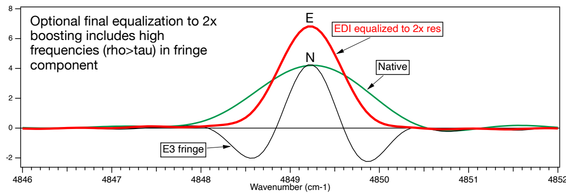

Figure 13. After crossfading discovers Δx and corrects raw data by −Δx, an optional final step is to recompute EDI output with equalization (filtering sum of native and raw fringing signal to reduce ringing) that produces an ∼2x resolution boost. (Example single delay resolution boosting was performed on the Lick Hamilton echelle spectrograph in 2002.[6])

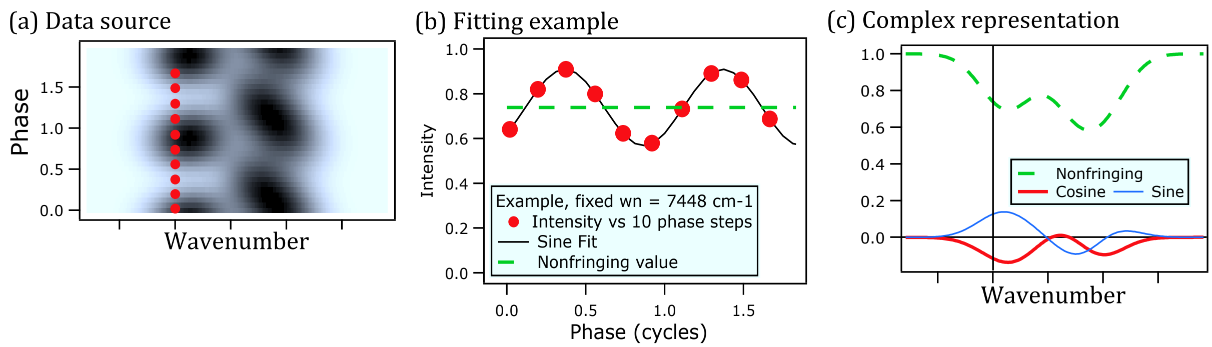

Figure 14. How to convert a set of phase stepped exposures into fringing and nonfringing spectra. (A set of phase stepped exposures of a spectrum is first stacked so each row in [a] is an exposure. Here we have ten rows but it can be as few as three.) Vertical lineout (a) across multiphase stack for a given wavenumber produces an intensity versus phase plot (b), which is fitted to a sinusoid (black curve). (c) The sine and cosine amplitudes (red and blue curves) are the whirl's (**W**) imaginary and real complex values, for a given wavenumber. The vertical offset of the fit is the ordinary spectrum (green, B_{ord}) at that wavenumber. Figure and caption reproduced with permission from Ref. 11 by SPIE.

8. APPENDIX: USEFUL INTERFEROMETER EQUATIONS

8.1 Interferometer transmission equation and useful variables

A line feature in the input spectrum will be measured by an EDI to produce in its output spectrum a wavelet. This is because EDI has a sensitivity limited to a Gaussian like peak in frequencies centered at the interferometer delay τ, the optical pathlength difference between interferometer arms, measured in units of cm. For interferometers the convenient unit along the dispersion direction is wavenumber (ν), in units cm^{-1}, since the sinusoidal transmission function of an interferometer

$$T(\nu) = (1/2)[1 + \cos(2\pi\tau\nu + \phi)]. \tag{1}$$

is linear in ν, where fringe phase offset ϕ is calibrated by a known spectral feature such as a ThAr lamp line. (The ν-dependence of τ due to glass refractive index dispersion is not time dependent and is calibrated away with ThAr measurements, as in Sect. 9 of Ref. 16) Frequencies (ρ) along the dispersion direction of features per cm^{-1}, are in units of cm, the same as delay τ, and the frequency of the sine comb is set by $\rho = \tau$.

8.2 Separating phase stepped data into fringing and nonfringing signals

(The equations and some sentences below come from Sect. 2 of Ref. 11.) The generic expressions for the fringing (**W**) and nonfringing (B_{ord}) spectra from a set of phase step exposures (B_n), where many (N) regular phase steps fit evenly around a circle ($\phi_n = n/N$, in units of cycles) are

$$\mathbf{W}(\nu) = \frac{1}{N}\sum B_n\, e^{-i2\pi\phi_n}\ , \tag{2}$$

$$B_{ord}(\nu) = \frac{1}{N}\sum B_n\ , \tag{3}$$

Our group sometimes calls the fringing spectra $\mathbf{W}(\nu)$ a "whirl". The nonfringing $B_{ord}(\nu)$ spectra is also called a "native", "ordinary", or "conventional" spectra. Note the similarity of Eq. 2 to a discrete Fourier transform which evaluates the sine and cosine amplitudes. Hence, an equivalent way of extracting the fringing and nonfringing components is to use a sine fitting routine along the phase axis, where for each pixel along the dispersion axis the height of the nonfringing component vs ν yields the nonfringing spectra $B_{ord}(\nu)$, and the sine and cosine amplitudes of the fit can be assigned to the imaginary and real parts of the fringing spectra $\mathbf{W}(\nu)$.

However, the phase steps will change across the band, since a given commanded delay increment $\Delta\tau$ at the interferometer mirror by the PZT transducer will elicit different phase shifts as $\Delta\phi = \Delta\tau/\lambda = \nu\Delta\tau$, and mechanical or air pressure changes (eg. due to wind at the dome) can also change the phase step from the commanded value. Our software assumes the phase steps are only approximately known and solves for the precise value in an iterative process. Hence we can measure fringing spectra across all orders of a very wide bandwidth echelle.

8.2.1 Writing code to separate fringing from nonfringing

The reader can write an algorithm for separating Fringing and Nonfringing components from a set of phase stepped exposures. (a) Starting with a sine fitting process along the phase independent variable (Fig. 14), initially assume a uniform commanded phase step to obtain a fit to $\mathbf{W}(\nu)$ and $B_{ord}(\nu)$, for each ν pixel. (b) Then using this fitted result for $\mathbf{W}(\nu)$ along the ν independent variable, for each phase exposure solve for a more precise value for the phase step value that brings it into better agreement with $\mathbf{W}(\nu)$, averaged over all ν. Hence the independent variable of the analysis alternates between phase, and then the dispersion variable. Then repeat the pair of steps (a)(b) iteratively.

One can start with a small bandwidth for the initial iteration, and then widen it. For the very wide bandwidth of an echelle spectrograph where λ may change over the orders by, say a factor of 1.5x from short to long wavelengths, some of the phase steps will be highly constrained when forced to be consistent over the entire bandwidth of phase stepping behavior, given that the final phase step may not wrap around the phase circle for the short wavelength, but for the long wavelength this same phase step can wrap around the circle significantly. Hence a unique and precise answer to the phase steps can be obtained when the full bandwidth of the spectrograph system is utilized. (We did not need to use this power of the full bandwidth, and for expediency we only used the bandwidth of a single order [of several] in the TripleSpec data.)

ACKNOWLEDGMENTS

Thanks for help with the TEDI project on Mt. Palomar Observatory from many colleagues, including James Lloyd, Phil Muirhead and Matthew Muterspaugh. Thanks to more recent guidance from Dayne Fratanduono, Eric Linder, L. L. LoDestro, Jon Eggert, Richard Ozer, Emma Floyd, and Alan Chew. High-resolution spectra of a ThAr lamp provided by Florian Kerber (NIST). Portions of work performed under the auspices of the U.S. Department of Energy by Lawrence Livermore National Laboratory under Contract DE-AC52-07NA27344, and by Laboratory Directed Research and Development project 22-LW-020, and based upon prior work supported by the National Science Foundation under Grant No. AST-0505366, AST-096064, PAARE AST-1059158, NASA Grant NNX09AB38G.

REFERENCES

[1] Erskine, D. J., "Combined dispersive/interference spectroscopy for producing a vector spectrum," *US Patent* **6,351,307** (Issued Feb. 26, 2002).

[2] Erskine, D. J., "Techniques in broadband interferometry," Tech. Rep. UCRL-TR-201695, Lawrence Livermore Nat. Lab. (Jan 2004); https://doi.org/10.2172/15009760.

[3] Erskine, D. J. and Ge, J., "Novel Interferometer Spectrometer for Sensitive Stellar Radial Velocimetry," in [*Imaging the Universe in Three Dimensions: Astrphys. Advncd. Multi-Wavel. Imaging Devices*], van Breugel, W. and Bland-Hawthorn, J., eds., *ASP Conf. Series* **195**, 501–507 (Jan. 2000); http://digital.library.unt.edu/ark:/67531/metadc780974/.

[4] Ge, J., Erskine, D. J., and Rushford, M., "An Externally Dispersed Interferometer for Sensitive Doppler Extrasolar Planet Searches," *PASP* **114**, 1016–1028 (Sept. 2002).

[5] Erskine, D. J., "An Externally Dispersed Interferometer Prototype for Sensitive Radial Velocimetry: Theory and Demonstration on Sunlight," *PASP* **115**, 255–269 (Feb. 2003); https://doi.org/10.1086/345995.

[6] Erskine, D. J., Edelstein, J., Feuerstein, W. M., and Welsh, B., "High-Resolution Broadband Spectroscopy Using an Externally Dispersed Interferometer," *ApJ* **592**, L103–L106 (Aug. 2003); https://doi.org/10.1086/377703.

[7] Erskine, D. J. and Edelstein, J., "Interferometric resolution boosting for spectrographs," in [*Ground-based Instrumentation for Astronomy*], Moorwood, A. and Iye, M., eds., *Proc. SPIE* **5492**, 190–199 (2004).

[8] Erskine, D. J., Edelstein, J., Lloyd, J., and Muirhead, P., "Noise studies of externally dispersed interferometry for Doppler velocimetry," in [*Ground-based and Airborne Instrumentation for Astronomy*], McLean, I. and Iye, M., eds., *Proc. SPIE* **6269** (2006).

[9] Muirhead, P. S., Edelstein, J., Erskine, D. J., Wright, J. T., Muterspaugh, M. W., Covey, K. R., Wishnow, E. H., Hamren, K., Andelson, P., Kimber, D., Mercer, T., Halverson, S. P., Vanderburg, A., Mondo, D., Czeszumska, A., and Lloyd, J. P., "Precise Stellar Radial Velocities of an M Dwarf with a Michelson Interferometer and a Medium-Resolution Near-Infrared Spectrograph," *PASP* **123**, 709 (June 2011).

[10] Erskine, D. J., Edelstein, J., Wishnow, E. H., Sirk, M., Muirhead, P. S., Muterspaugh, M. W., Lloyd, J. P., Ishikawa, Y., McDonald, E. A., Shourt, W. V., and Vanderburg, A. M., "High-resolution broadband spectroscopy using externally dispersed interferometry at the Hale telescope: part 1, data analysis and results," *Journal of Astronomical Telescopes, Instruments, and Systems* **2**, 025004 (Apr. 2016); https://doi.org/10.1117/1.JATIS.2.2.025004.

[11] Erskine, D. J., Edelstein, J., Wishnow, E., Sirk, M., Muirhead, P. S., Muterspaugh, M. W., and Lloyd, J. P., "High-resolution broadband spectroscopy using externally dispersed interferometry at the Hale telescope: part 2, photon noise theory," *Journal of Astronomical Telescopes, Instruments, and Systems* **2**, 045001 (Oct. 2016).

[12] Erskine, D. J., Muirhead, P. S., Vanderburg, A. M., and Szentgyorgyi, A., "Enhanced exoplanet biosignature detection from an interferometer addition to low resolution spectrographs," in [*Ground-based and Airborne Instrumentation for Astronomy VII*], Evans, C. J., Simard, L., and Takami, H., eds., *Society of Photo-Optical Instrumentation Engineers (SPIE) Conference Series* **10702**, 107024G (July 2018).

[13] Erskine, D. J., "Dispersed interferometers," in [*The WSPC Handbook of Astronomical Instrumentation*], Burrows, D. N., ed., **Vol. 3**, World Scientific, Singapore, ISBN = 978-981-4644-31-0 (June 2021). doi.org/10.1142/9446.

[14] Erskine, D. J., "Method for boosting dispersive spectrograph stability 1000x using interferometry with crossfaded pairs of delays," *Journal of Astronomical Telescopes, Instruments, and Systems* **7**, 025006 (June 2021); https://doi.org/10.1117/1.JATIS.7.2.025006.

[15] Erskine, D. J., "Spectrograph Stabilization using a Single-delay Interferometer," *US Patent* **12,480,815** (Issued Nov. 25 2025).

[16] Erskine, D. J., Edelstein, J., Wishnow, E. H., Sirk, M. M., Linder, E. V., and Fratanduono, D. E., "Spectrograph stabilization using a single-delay interferometer on the Hale Telescope," *Journal of Astronomical Telescopes, Instruments, and Systems* **12**(2), 025006 (2026); https://doi.org/10.1117/1.JATIS.12.2.025006.

[17] Ge, J., van Eyken, J., Mahadevan, S., DeWitt, C., Kane, S. R., Cohen, R., Vanden Heuvel, A., Fleming, S. W., Guo, P., Henry, G. W., Schneider, D. P., Ramsey, L. W., Wittenmyer, R. A., Endl, M., Cochran, W. D., Ford, E. B., Martín, E. L., Israelian, G., Valenti, J., and Montes, D., "The first extrasolar planet discovered with a new-generation high-throughput Doppler instrument," *ApJ* **648**, 683–695 (2006).

[18] Ma, B., Ge, J., Wolszczan, A., Muterspaugh, M. W., Lee, B., Henry, G. W., Schneider, D. P., Martín, E. L., Niedzielski, A., Xie, J., Fleming, S. W., Thomas, N., Williamson, M., Zhu, Z., Agol, E., Bizyaev, D., da Costa, L. N., Jiang, P., Fiorenzano, A. F. M., Hernández, J. I. G., Guo, P., Grieves, N., Li, R., Liu, J., Mahadevan, S., Mazeh, T., Nguyen, D. C., Paegert, M., Sithajan, S., Stassun, K., Thirupathi, S., van Eyken, J. C., Wan, X., Wang, J., Wisniewski, J. P., Zhao, B., and Zucker, S., "Very low-mass stellar and substellar companions to solar-like stars from MARVELS. VI. a giant planet and a brown dwarf candidate in a close binary system HD 87646," *Astronomical Journal* **152**, 112 (Oct. 2016). 10.3847/0004-6256/152/5/112.

[19] van Eyken, J. C., Ge, J., and Mahadevan, S., "Theory of Dispersed Fixed-delay Interferometry for Radial Velocity Exoplanet Searches," *ApJS* **189**, 156–180 (2010).

[20] van Eyken, J. C., Ge, J., Mahadevan, S., and DeWitt, C., "First Planet Confirmation with a Dispersed Fixed-Delay Interferometer," *ApJ* **600**, L79–L82 (2004).

[21] Kim, A. G., Linder, E. V., Edelstein, J., and Erskine, D., "Giving cosmic redshift drift a whirl," *Astroparticle Physics* **62**, 195–205 (Mar. 2015).

[22] Wilson, J. C., Henderson, C. P., Herter, T. L., Matthews, K., Skrutskie, M. F., Adams, J. D., Moon, D.-S., Smith, R., Gautier, N., Ressler, M., Soifer, B. T., Lin, S., Howard, J., LaMarr, J., Stolberg, T. M., and Zink, J., "Mass producing an efficient NIR spectrograph," in [*Ground-based Instrumentation for Astronomy*], Moorwood, A. and Iye, M., eds., *Proc. SPIE* **5492**, 1295–1305 (2004).

[23] Kerber, F., Nave, G., and Sansonetti, C. J., "The Spectrum of Th-Ar Hollow Cathode Lamps in the 691-5804 nm region: Establishing Wavelength Standards for the Calibration of Infrared Spectrographs," *ApJS* **178**, 374–381 (2008).

[24] Milaković, D. and Jethwa, P., "A new method for instrumental profile reconstruction of high-resolution spectrographs," *Astronomy & Astrophysics* **684**, A38 (Apr. 2024).

[25] Milaković, D., Pasquini, L., Webb, J. K., and Lo Curto, G., "Precision and consistency of astrocombs," *Monthly Notices of the Royal Astronomical Society* **493**, 3997–4011 (02 2020).

[26] Fischer, D. A., Anglada-Escude, G., Arriagada, P., et al., "State of the Field: Extreme Precision Radial Velocities," *Proc. Astr. Soc. Pacific* **128**, 066001 (June 2016).

[27] Erskine, D., Buschmann, M., Easther, R., Ferraro, S., Kim, A., Linder, E., Muirhead, P., Phillips, D., Ravi, A., Safdi, B., Schaan, E., Silverwood, H., and Walsworth, R., "Direct Acceleration: Cosmic and Exoplanet Synergies," *Bulletin of the American Astronomical Society* **51**, 53 (May 2019).

[28] Mahadevan, S., Ge, J., Fleming, S. W., Wan, X., DeWitt, C., van Eyken, J. C., and McDavitt, D., "An inexpensive field-widened monolithic michelson interferometer for precision radial velocity measurements," *PASP* **120**, 1001–1015 (2008).

[29] Wan, X. and Ge, J., "Monolithic Michelson Interferometer as ultra stable wavelength reference," in [*Optical and Infrared Interferometry II*], Danchi, W. C., Delplancke, F., and Rajagopal, J. K., eds., **7734**, 77343N, International Society for Optics and Photonics, SPIE (2010).

[30] Wan, X., Ge, J., and Chen, Z., "Development of stable monolithic wide-field michelson interferometers," *Appl. Opt.* **50**, 4105–4114 (Jul 2011).

[31] Wang, J., Ge, J., Wan, X., De Lee, N., and Lee, B., "Accurate Group Delay Measurement for Radial Velocity Instruments Using the Dispersed Fixed Delay Interferometer Method. II. Application of Heterodyne Combs Using an External Interferometer Filter," *PASP* **124**, 1159 (Oct. 2012).

[32] Xiaoke Wan and Jian Ge, "Stable monolithic interferometer for wavelength calibration," *US Patent* **8,570,524** (Issued Oct. 29, 2013).

[33] Malitson, I. H., "Interspecimen comparison of the refractive index of fused silica," *J. Opt. Soc. Am.* **55**, 1205–1209 (Oct 1965).

[34] Hahn, T. A. and Kirby, R. K., "Thermal Expansion of Fused Silica from 80 to 1000 K Standard Reference Material 739," *AIP Conference Proceedings* **3**, 13–24 (01 1972).